


The Antitumor Impact of Combining Hepatic Artery Ligation With Copper Chelators for Liver Cancer

Ni Zeng^{1*}, Ye Wang^{2*}, Yuan Wan^{3*}, Hongyu Wang⁴
and Nan Li⁵ 

Clinical Medicine Insights: Oncology
Volume 17: 1–8
© The Author(s) 2023
Article reuse guidelines:
sagepub.com/journals-permissions
DOI: 10.1177/11795549231204612



¹Center for Translational Medicine, Institute of Precision Medicine, The First Affiliated Hospital, Sun Yat-sen University, Guangzhou, China. ²School of Medicine, South China University of Technology, Guangzhou, China. ³Interventional Center, The Sixth Affiliated Hospital of Sun Yat-Sen University, Guangzhou, China. ⁴Department of Interventional Therapy, Guangdong Provincial Hospital of Chinese Medicine and Guangdong Provincial Academy of Chinese Medical Sciences, Guangzhou, China. ⁵Department of Interventional Radiology, Guangzhou First People's Hospital, Guangzhou, China.

ABSTRACT

BACKGROUND: Hepatocellular carcinoma (HCC) is one of the main cancer-related mortality worldwide. Thus, there is a constant search for improvement in treatment strategies to enhance the prognosis of this malignancy. The study aims to investigate the combined antitumor activity of ammonium tetrathiomolybdate (TM, copper chelator) combined with hepatic artery ligation (HAL) for liver cancer.

METHODS: A total of 40 Sprague-Dawley (SD) rats bearing hepatic tumors were randomly divided into four groups: the control group without any treatment (control), HAL only (HAL), given TM by gavage (TM), and given TM combined with HAL (HAL + TM). The concentrations of serum copper were measured at the predetermined time points. Tumor growth rate, overall survival (OS), expression of hypoxia-inducible factor-1 α (HIF-1 α), vascular endothelial growth factor (VEGF), and microvessel density (MVD), as determined by immunohistochemical examination, were compared.

RESULTS: HAL treatment transiently could elevate alanine transaminase (ALT) and aspartate transaminase (AST) but resumed to baseline within 1 week. Serum copper was significantly increased in tumor-bearing animals over time. The values of serum copper in the three treatment groups were significantly lower than those in the control group at different time points, with the lowest values observed in the TM group ($P < .05$). The average tumor size was 30.33 ± 2.58 , 20.83 ± 2.93 , 16.80 ± 3.84 , and 10.88 ± 1.08 mm in the control, HAL, TM, and HAL + TM groups, respectively (HAL + TM vs other groups, all $P < .05$). In addition, the expression levels of HIF-1 α , VEGF, and MVD were significantly lower in the HAL + TM group than those in the other groups ($P < .05$). The OS of rats in the combined groups was significantly prolonged compared to the other groups ($P < .05$), with survival time of 19.1 ± 0.64 , 25.4 ± 1.24 , 25.3 ± 1.78 , and 29.9 ± 2.22 days in the control, HAL, TM, and HAL + TM groups, respectively.

CONCLUSION: These findings suggest that combined treatment with TM and HAL holds great potential for liver cancer treatment by reducing tumor hypoxia and angiogenesis. The observed results indicate that these combinations may offer a novel target and strategy for interventional therapy of liver cancer.

KEYWORDS: Liver tumor, copper, copper chelator, transarterial embolization, combination therapy, tumor angiogenesis

RECEIVED: March 14, 2023. ACCEPTED: September 13, 2023.

TYPE: Original Research Article

CORRESPONDING AUTHOR: Nan Li, Department of Interventional Radiology, Guangzhou First People's Hospital, Guangzhou 510180, China.
Email: zsylinan@163.com

Introduction

HCC, one of the most common solid malignancies, is a leading cause of cancer-related death worldwide, and most patients present with advanced stages of this disease with the dismal prognosis.^{1–3} Transarterial embolization (TAE) has been adopted as the standard of care for advanced HCC patients.^{4–7} However, the overall prognosis for patients undergoing TAE varies considerably due to the high heterogeneity of HCC and hypoxia post-TAE which can further stimulate angiogenesis.^{8–13} Hence, the concept to enhance the therapeutic effect of TAE and

improve the benefit of patients is being addressed using tyrosine kinase inhibitors, such as sorafenib or lenvatinib.^{3,14} Nevertheless, the improvements in patient outcomes have been modest.¹⁴ Targeting 1 or 2 proteins in the complex cancer cascade has been proven to be insufficient in controlling cancer growth.^{15,16} Therefore, novel therapies for HCC remain an unmet medical need.

Copper (Cu) is an essential micronutrient involved in various fundamental biological processes. Recent findings have established a correlation between elevated Cu levels in serum and tissue and the progression of several malignancies, including lymphoma, reticulum cell sarcoma, cervical, breast,

*N.Z., Ye.W., and Yu.W. contributed equally to this article.



stomach, and lung cancers.¹⁷⁻²³ Our previous study demonstrated that high serum copper promotes liver cancer progression, while copper chelators suppress tumor growth.²⁴ Moreover, the use of copper chelators to decrease copper bioavailability has been extensively investigated in clinical studies as a strategy to inhibit angiogenesis in multiple cancer types, including metastatic cancer, malignant pleural mesothelioma, and esophageal cancer.²⁵⁻³² Therefore, whether the combination of TAE and copper chelator can effectively control HCC angiogenesis and tumor growth needs to be explored further. Hence, the objective of this study was to investigate the maximal antitumor activity of copper chelators combined with TAE for liver cancer.

Materials and Methods

Animals and materials

Walker-256 tumor cells were purchased from Cellcook Biotech Co., Ltd (Guangzhou, China). Anti-VEGF antibody (rabbit monoclonal IgG, 1:200 dilution, Cat. no. ab32152) was purchased from Abcom Inc. HIF-1 α (rabbit polyclonal IgG, 1:100 dilution, Cat. no. GB13031-1) and CD34 (rabbit polyclonal IgG, 1:200 dilution, GB13013) were purchased from Servicebio Technology CO., LTD (Wuhan, China). Ammonium TM (99.95%) (Cat. no. G1915025) was purchased from Aladdin Biochemical Technology Co., Ltd (Shanghai, China).³³ Four-week-old BALB/c nude mice (body weight = 12-15 g; n = 8) which were used as Walker-256 tumor-bearing donor mice at a site on the lateral thigh and male SD rats aged 5 to 7 weeks (body weight = 150-200 g; n = 60) were purchased from Guangdong Medical Laboratory Animal Center (Guangzhou, China) and Laboratory Animal Center of Sun Yat-sen University (Guangzhou, China), and maintained in the Laboratory Animal Center of Sun Yat-sen University under specific pathogen-free (SPF) conditions and were allowed free access to food and water throughout the acclimation and experiment protocols.³⁴ All animal procedures were performed according to approved protocols (No: SYSU-IACUC-2020-000209) and in accordance with the recommendations for the proper care and use of laboratory animals.

Animal treatments

To establish the xenograft model, Walker-256 tumor cells (1×10^6 cells) were injected into the flank of nude mice, following an established protocol.³⁵ When the tumor size reached approximately 8 to 10 mm 10 days after injection, the subcutaneous tumors were minced into 1.0 mm³ cubes for subsequent experiments. Subsequently, an *in situ* liver cancer procedure was performed on SD rats. The rats were laparotomized by making a midline abdominal incision under intraperitoneal anesthesia with 3% pentobarbital sodium at a dose of 50 mg/kg under

sterile conditions. In the abdominal cavity, the accessory left liver lobe was protruded laterally, and a subcapsular tunnel was created using 22-gauge short-beveled needles. Next, a fish-like fleshy tumor tissue cube was inserted into the tunnel using the needle, and the wound was covered by a small piece of gelfoam in case of hemorrhage. Then, the rats were promptly returned to their home cages to recover after surgery and regain normal activity the next day.

The HAL procedure was performed 10 days of implantation by two experienced surgeons.³⁶ In brief, each rat's liver was exposed through laparotomy under anesthesia using pentobarbital sodium, and then, the hepatic artery was identified by lifting up the liver with gauze under zoom stereo microscope. Subsequently, the left hepatic artery was then isolated from the portal vein and common bile duct. A suture was placed under the left hepatic artery and then ligated. Finally, the laparotomy wound was closed, and the rats were immediately returned to their home cages for recovery.

After 10 days of implantation and 10 days of HAL, liver tumor models were evaluated and analyzed using 3.0T magnetic resonance imaging (MRI) (Vida; Siemens). The main scanning parameters were as follows: repetition time (TR) = 700 milliseconds and echo time (TE) = 13 milliseconds for T1-weighted image (T₁WI); TR = 2000 milliseconds and TE = 53 milliseconds for T2-weighted image (T₂WI) (slice thickness = 2 mm). The growth of the tumor was plotted using a graph based on tumor size and time of implantation.

The 40 rats with established xenograft tumor were randomly allocated into four groups with 10 rats in each group. The groups were as follows: control group: the control group without any treatment; HAL group: HAL only; TM group: given TM at a dose of 1.25 mg/day once daily by gavage;^{24,37} and HAL + TM group: given TM combined with HAL. TM was administered for 7 days. Left HAL was performed to simulate TAE.

Pathological investigations

Blood samples were collected from 5 normal rats and 24 rats with liver cancer at various time points: right before implantation, pre-TAE, and 1, 3, and 7 days post-TAE treatment, respectively. The therapeutic safety was assessed by liver enzymes including alanine aminotransferase (ALT, U/L) and aspartate aminotransferase (AST, U/L). Then, serum copper concentrations were quantified using inductively coupled plasma mass spectrometry (ICP-MS) (Agilent 7700x ICP-MS spectrometer, Agilent Technologies, Germany).^{24,38} Tumor tissues were excised from the rats after their natural death. Some tumors were fixed in 4% paraformaldehyde for histologic examination and immunohistochemistry (IHC).

The remaining tumor samples were embedded in paraffin, sectioned into 3- μ m sections, dewaxed, rehydrated using xylene

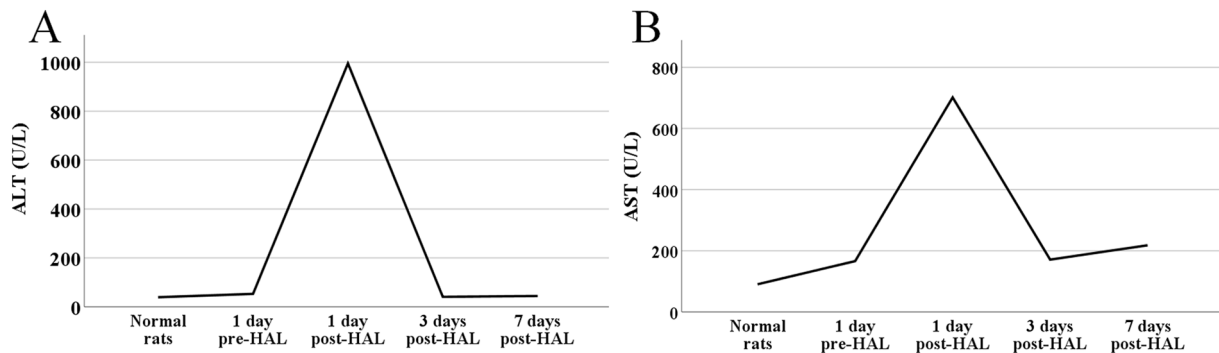


Figure 1. (A) Changes of ALT and (B) AST before and after HAL treatment. $P > .05$ for day 1 pre-HAL treatment versus day 7 post-HAL treatment in examinations.

ALT indicates alanine aminotransferase; AST, aspartate aminotransferase; HAL, hepatic artery ligation.

and successive ethanol baths, immersed in 10 mM Tris and 0.5 M ethylene diamine tetraacetic acid at pH 9.0, and then microwaved twice for 5 minutes each. Subsequently, the sections were incubated with 3% H_2O_2 for 10 minutes to block endogenous peroxidase activity. The sections were then incubated overnight at 4 °C with specific primary antibodies (dilutions: VEGF, 1:200; CD34, 1:200; HIF-1 α , 1:100) in a humidified atmosphere for 15 minutes. After 15 minutes, slides were washed with freshly prepared phosphate buffer saline (PBS) 3 times for 3 minutes each. Slides were then incubated with a secondary antirabbit immunoglobulin and then washed with phosphate buffer saline (PBS) 3 times for 3 to 5 minutes each. The sections were scanned using a Leica Aperio AT2 (Leica Biosystems, Germany) scanner, and the images were analyzed using ImageJ software.

The expression of VEGF and MVD was independently reviewed by two experienced pathologists who were blinded to every slide. The expression of VEGF was determined by counting stained epithelial cells in five random sights on each slide (400 magnification) as previously described.³⁵ Intratumoral MVD was assessed using the vascular hotspot technique described by Weidner *et al.*^{35,39} Briefly, sections were initially scanned at low power to identify regions with the highest vascular density, and stained microvessels were then counted in five separate random fields at high power (400 magnification) within this region. The mean number of microvessels per field was calculated as the MVD for each group. The percentage of HIF-1 α expression for the entire tumor sample was calculated by dividing the area of positive HIF-1 α staining by the sum of the stained and unstained areas of the tumor cells. Necrotic cells were excluded from the calculation, as they are already nonviable and do not express HIF-1 α .⁴⁰

Data analysis

The results were calculated by averaging data from multiple measurements and were presented as mean \pm standard deviation. One-way analysis of variance (ANOVA) complemented with Student's *t* test using statistical product and service solutions software package (version 25.0) for differences

between means was used to detect any significant difference ($P < .05$) of VEGF and MVD among different groups in this study. The Mann-Whitney U test was used to compare the mean percentage of HIF-1 α -positive stained cells among different groups.

Result

Therapeutic safety

In this study, the safety of HAL treatment was assessed based on the levels of alanine aminotransferase (ALT) and aspartate aminotransferase (AST) in the serum. The result indicated that after HAL treatment, there was an elevation in the levels of serum liver. Specifically, there was a significant increase in ALT (>14 times) and AST (>5 times) at 1 day post-HAL compared with 1 day pre-HAL (ALT, 995.08 ± 870.22 vs 52.77 ± 16.87 U/L, $P < .01$; AST, 701.69 ± 984.93 vs 166 ± 63.95 U/L, $P < .001$, respectively). However, these enzyme levels subsequently returned to baseline within 1 week, similar to the levels observed in normal rats (ALT, 39.2 ± 3.63 U/L; AST, 90.4 ± 12.52 U/L) and rats' pre-HAL treatment (Figure 1). These findings suggest that HAL treatment is a safe strategy without evident hepatic toxicity.

Change of serum copper concentration

To investigate the impact of the tumors on serum copper, we assessed the serum copper levels in healthy rats and liver cancer rats at different time points. As depicted in Figure 2, liver cancer rats exhibited higher serum copper levels at 9 days after implantation (1385.62 ± 178 μ g/L) and 17 days after implantation (3095.53 ± 316.83 μ g/L) when compared with the levels observed in normal healthy individuals (778.44 ± 54.12 μ g/L) with statistical significance ($P < .01$), thereby suggesting a substantial elevation of serum copper in tumor-bearing animals over the course of tumor inoculation.

In addition, the serum copper concentrations were 1359.3 ± 333.67 , 1143.67 ± 215.05 , and 1265.47 ± 150.1 μ g/L, respectively, among the three treatment groups (TM, HAL, and HAL + TM) 1 day before HAL treatment. The serum

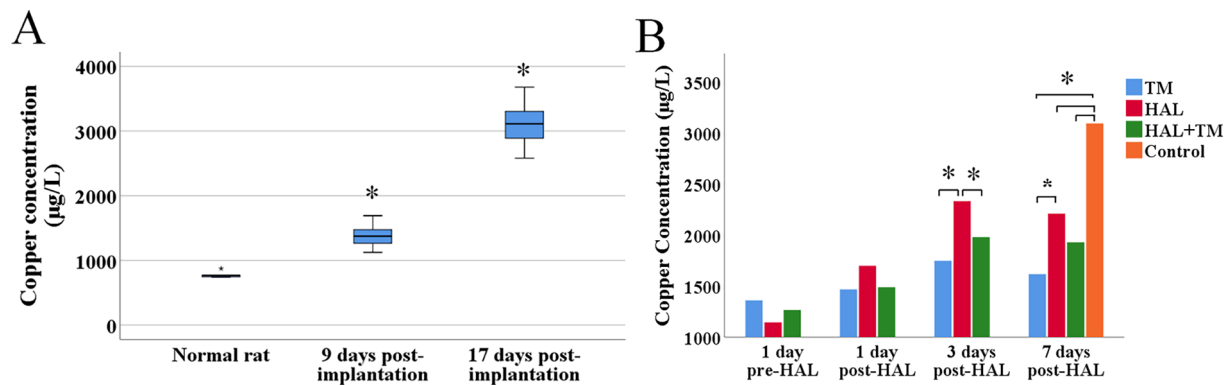


Figure 2. Serum copper level of healthy normal and liver carcinoma-bearing rat at different time points. (A) The serum copper levels in healthy rats and liver cancer rats at 9 and 17 days after implantation ($*P < .05$ between each two time points). The whiskers represent the 5th to 95th percentile range. (B) The serum copper concentration on different groups at different time points. ($*P < .05$ between two groups shown by horizontal line).

copper concentration at 1, 3, and 7 days after treatment was (1441.41 ± 120.42 , 1698.07 ± 238.29 , 1488.2 ± 194.32), (1685.31 ± 203.1 , 2332.21 ± 250.25 , 1979.23 ± 290.32), and (1615.87 ± 186.18 , 2210.03 ± 218.89 , 1928.7 ± 317.39) $\mu\text{g/L}$, respectively. No significant difference was observed in serum copper concentration between the three groups 1 day before and 1 day after HAL. However, significant differences become apparent between the HAL group and the other two treatment groups 3 days after HAL treatment. Furthermore, 7 days after the operation, the serum copper among the three treatment groups was significantly lower compared with the control group ($P < .05$).

Therapeutic efficacy

In this work, rat Walker-256 liver tumor models were successfully established for *in vivo* experiments as demonstrated by the imaging surveillance that tumor mass with a diameter of approximately 8 mm developed in the left liver lobe 10 days after implantation. The Walker-256 tumor in liver presented as a slightly hyperintense mass in $T_2\text{WI}$ without obvious demarcation between the tumor and surrounding normal liver tissue (Figure 3A and B). MR scan was again performed 10 days after the intervention, and the maximum diameter of the tumor was calculated according to the response evaluation criteria in solid tumors (RECIST) 1.1 criteria.⁴¹ As shown by MRI, the size of intrahepatic tumors showed a significant increase when compared with the baseline (8.6 ± 1.73 mm) ($P < .05$) (Figure 3). The size of the tumor in the control, HAL, TM, and HAL + TM groups was 30.33 ± 2.58 , 20.83 ± 2.93 , 16.80 ± 3.84 , and 10.88 ± 1.08 mm, respectively (Figure 3C), (control vs HAL, TM, and HAL + TM), all $P < .05$; (HAL and TM) vs (HAL + TM), all $P < .05$; HAL vs TM, $P > .05$.

As shown in Figure 4, the OS of rats with different treatments (25.4 ± 1.24 , 25.3 ± 1.78 , and 29.9 ± 2.22 days in groups HAL, TM, and HAL + TM, respectively) had a significantly prolonged OS than those in the control group (19.1 ± 0.64 days). The OS of rats in the HAL + TM group was the longest with

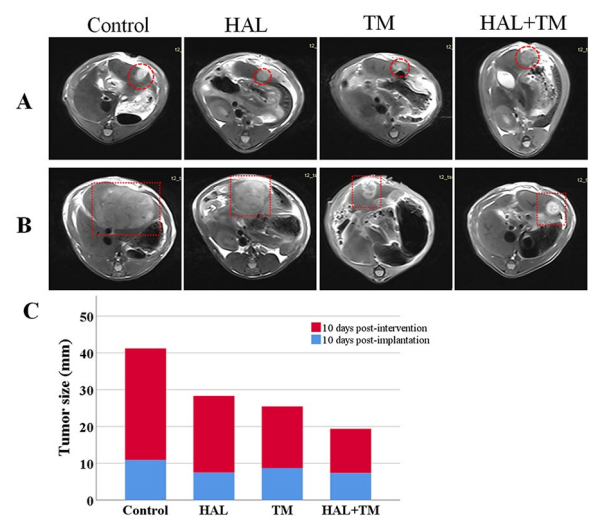


Figure 3. HAL combined with TM can inhibit tumor growth in rat liver cancer model. Representative axial $T_2\text{W}$ MR images of Walker-256 liver tumors at (A) 10 days after implantation and (B) at 10 days after different interventions. Red dotted squares indicated tumor locations. Tumors show increased signal intensity (arrows) relative to remaining liver. (C) Treatment response and the changes of the maximum tumor diameters of control and treatment groups compared with the baseline. HAL indicates hepatic artery ligation; MR, magnetic resonance; TM, tetrathiomolybdate.

statistical significance when compared with the other two treatment groups (HAL + TM vs HAL and TM, all $P < .05$), suggesting that TM combined with HAL have a good potential for liver cancer treatment.

Histologic features

The development, progression, and metastasis of solid tumors are closely related to angiogenesis. As key inducing factors of tumor angiogenesis, HIF-1 α , VEGF, and MVD are involved in all stages of HCC.⁴²

Walker-256 liver tumors exhibited a characteristic pattern of HIF-1 α -positive staining (Figure 5). The control group displayed the highest level of HIF-1 α staining ($85.57 \pm 8.6\%$).

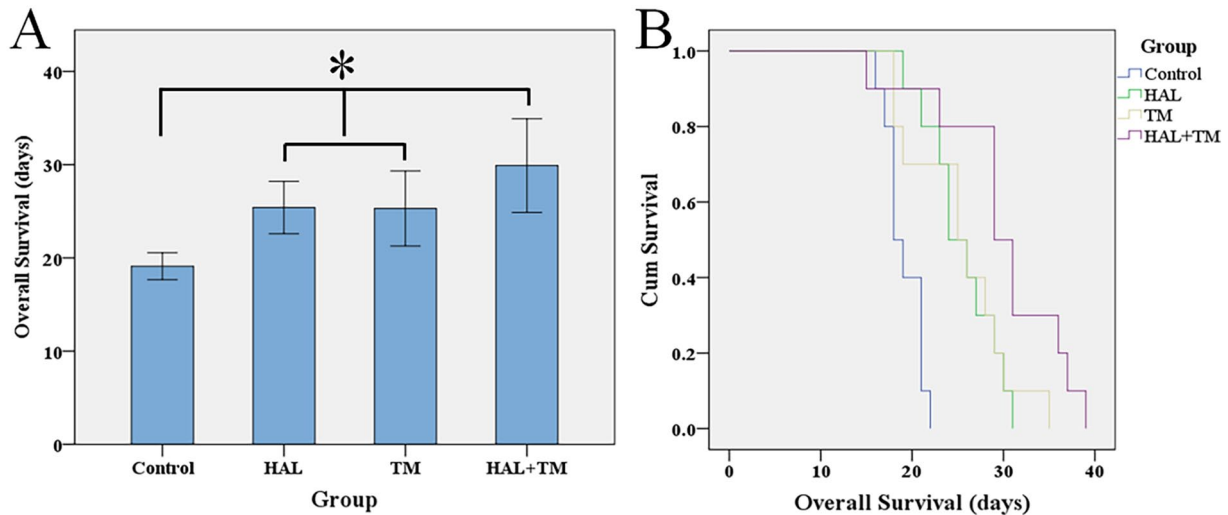


Figure 4. Kaplan-Meier curves were plotted to determine OS rates of rats with liver cancer based on different treatments. (A) Median survival time for the animals from all four groups. (* $P < .05$ among the groups shown by horizontal line). The whiskers represent the 5th to 95th percentile range. (B) Kaplan-Meier curves were plotted to determine OS rates of rats with liver cancer based on different treatments. HAL indicates hepatic artery ligation; OS, overall survival; TM, tetrathiomolybdate.

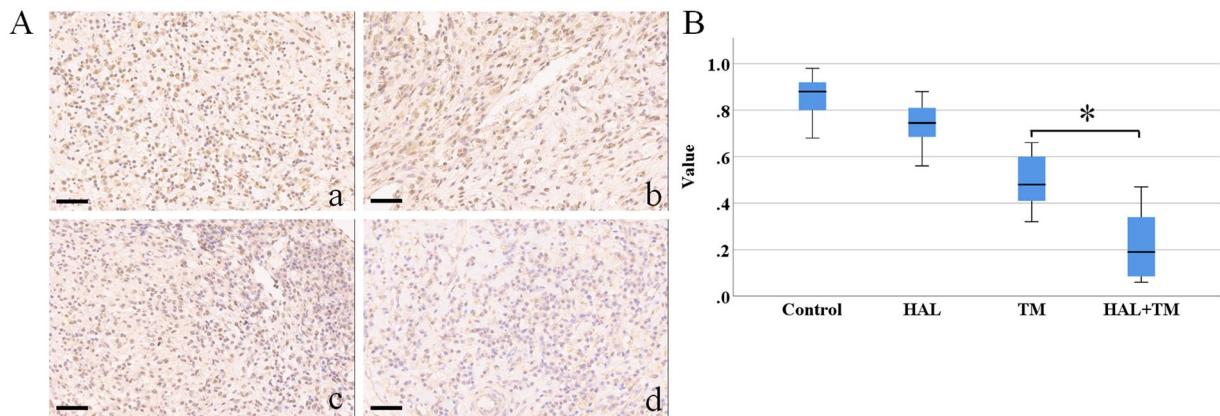


Figure 5. TM reduced hepatoma HIF-1 α overexpression combined with HAL in rat models. (A) Representative IHC staining for HIF-1 α expression on different groups (magnification $\times 400$). Scale bars are $50 \mu\text{m}$. (a) Control group, (b) HAL group, (c) TM group, and (d) HAL + TM group. (B) Quantitative results of HIF-1 α . * $P < .05$ between the horizontal two groups. The whiskers represent the 5th to 95th percentile range. HAL indicates hepatic artery ligation; HIF-1 α , hypoxia-inducible factor-1 α ; IHC, immunohistochemistry; TM, tetrathiomolybdate.

However, treatment with HAL and/or TM resulted in a significant decrease in the average percentage of HIF-1 α expression, which was $72.24 \pm 11.17\%$, $50.10 \pm 10.86\%$, and $21.74 \pm 14.71\%$ in the HAL, TM, and HAL + TM groups (all $P < .05$ between each two groups). Hepatic cancer VEGF expression appeared as brown staining in the cytoplasm (Figure 6). The control group (87.08 ± 14.83) exhibited a substantial increase in VEGF-positive vascular endothelial cells detected by IHC, with a mean value of 87.08 ± 14.83 . In contrast, the treatment groups showed significantly lower mean values: 63.16 ± 6.66 , 51.60 ± 8.03 , and 36.86 ± 5.83 in the HAL, TM, and HAL + TM groups, respectively (all $P < .05$ between each two groups). CD34-positive cells appeared as brown or dark-brown staining (Figure 7). The trend in MVD was consistent with that of VEGF in the control, HAL, TM,

and HAL + TM groups (70.41 ± 16.84 , 46.24 ± 6.56 , 34.74 ± 5.76 , and 22.54 ± 5.37 , respectively) with the statistical difference among each two groups (all $P < .05$).

Discussion

Currently, TAE has been widely used to treat advanced HCC.^{43,44,45} In this study, the procedure of left HAL was used to mimic the clinical situation of TAE.⁴⁶ TAE treatment is usually accompanied by the damage to the normal liver. Therefore, the safety evaluation of the TAE strategy for liver cancer is critically important. In addition, our results showed that serum ALT and AST levels transiently increased after treatment for most rats, and recovered to baseline at 3 days after TAE, suggesting that TAE does not cause permanent liver damage. TAE can block the blood supply of the artery of

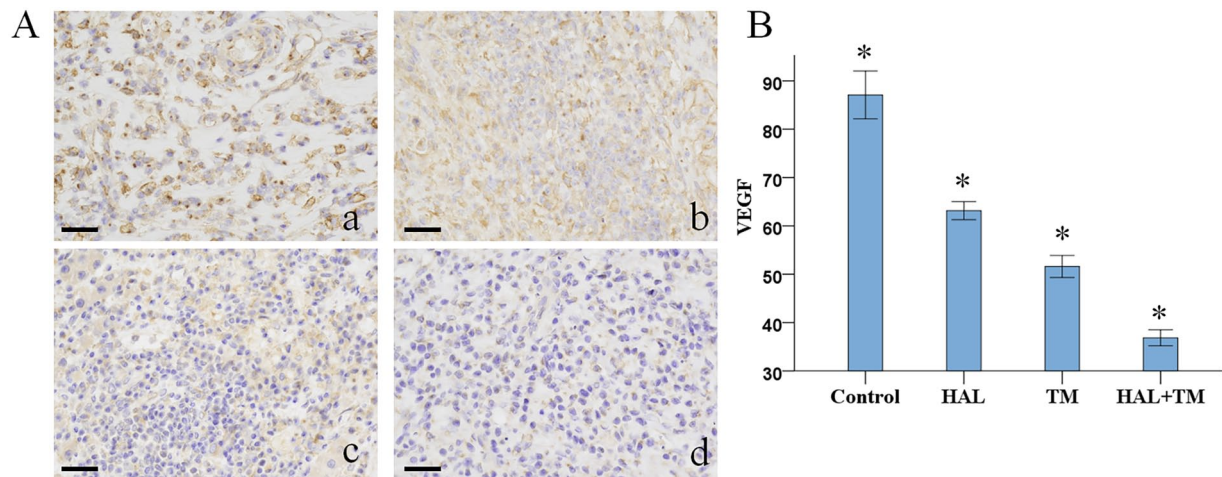


Figure 6. HAL and/or TM treatment in rats with implanted Walker-256 tumors depressed tumor angiogenesis. (A) Representative IHC staining for VEGF in different groups (magnification $\times 400$). Scale bars are $50\ \mu\text{m}$. (a) Control group, (b) HAL group, (c) TM group, and (d) HAL + TM group. (B) Quantitative results of VEGF. $*P < .05$ between each two groups. The whiskers represent the 5th to 95th percentile range. HAL indicates hepatic artery ligation; IHC, immunohistochemistry; VEGF, vascular endothelial growth factor; TM, tetrathiomolybdate.

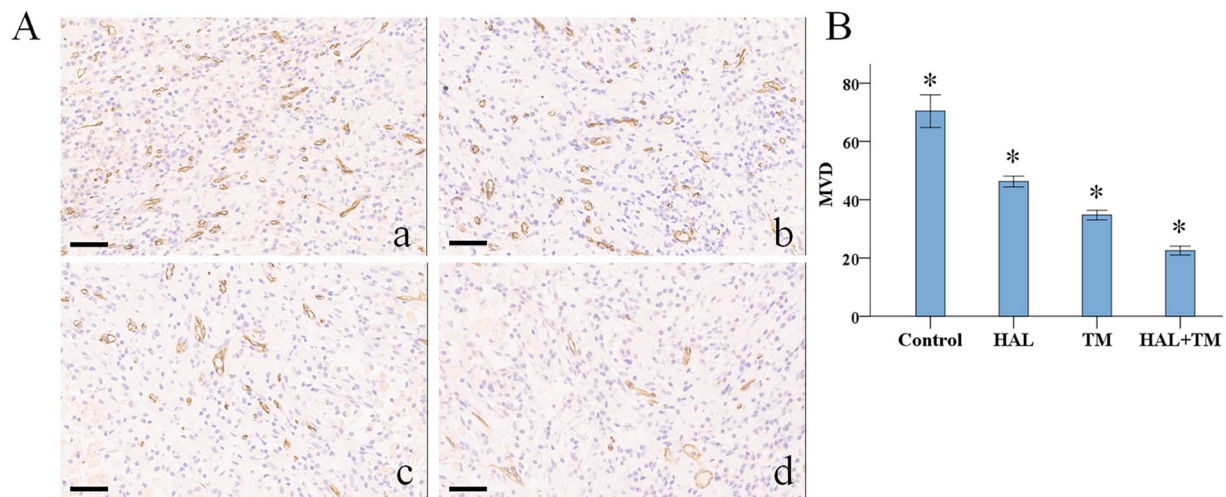


Figure 7. Combined TM and HAL reduced MVD in the rat models of liver cancer. (A) IHC staining of hepatoma MVD labeled by CD34 (magnification $\times 400$). CD34-positive endothelial cells or clearly separate clusters were counted as single microvessels. Scale bars are $50\ \mu\text{m}$. (a) Control group, (b) HAL group, (c) TM group, and (d) HAL + TM group. (B) Quantitative results of MVD. $*P < .05$ between each two groups. The whiskers represent the 5th to 95th percentile range. HAL indicates hepatic artery ligation; IHC, immunohistochemistry; MVD, microvessel density; TM, tetrathiomolybdate.

tumors, leading to necrocytosis eventually. Nonetheless, recent accumulating evidence has shown that hypoxic-ischemic condition post-TAE can activate the expression of HIF-1 α , which promotes the expression of VEGF and initiates tumor angiogenesis, finally resulting in treatment failure.⁴⁷⁻⁵⁰ Therefore, targeted suppression of hypoxia-mediated angiogenesis might hold a promising strategy against TAE failure.

Copper is considered as a “switch-on” angiogenic messenger, due to its ability to induce many proangiogenic responses and initiate tumor angiogenesis.⁵¹⁻⁵⁵ Consequently, copper chelators have garnered interest as potential antitumorogenic and antiangiogenic drugs, with investigations being conducted in both preclinical cancer models and clinical trials.^{26,56-59} In a recent study, we demonstrated that copper promotes tumor

progression, whereas copper chelators effectively suppress liver cancer growth.²⁴ This motivated us to undertake this study, aiming to explore the therapeutic effect of TAE combined with TM in the treatment of liver cancer.

The result indicated a significant increase in tumor size compared with the baseline. As anticipated, there was a notable reduction in tumor size among the groups treated with HAL + TM when compared with the other groups, suggesting that combination of HAL-TM inhibits tumor growth *in vivo*. In addition, rats treated with the combination therapy exhibited a significantly longer OS compared with the other groups. Collectively, these findings validate the superior therapeutic outcomes achieved with the combination of TM and HAL.

To explain these results, we propose the following mechanism: TAE blocks the blood supply of the tumor, while TM restricts copper availability diminishing the ability of known angiogenic factors to stimulate blood vessel development, which together effectively prevents cancer growth.¹⁸ In this study, we measured serum copper concentrations at different time points and different groups. The results demonstrated an elevation in copper concentration as tumor size increased, and notable tumor growth inhibition following the administration of TM, which aligns with the results of our previous study.²⁴ These findings suggest that copper promotes rapid tumor growth. Interestingly, a transient increase in serum copper was observed on day 3 following TAE, with the HAL + TM group exhibiting higher copper levels compared with the TM group. This may be attributed to liver injury after HAL. Furthermore, liver function indexes peaked on the third day and gradually recovered thereafter, indicating a decreased ability to metabolize copper during the liver function recovery period. Given that angiogenesis following TAE leads to treatment failure,⁴⁷⁻⁵⁰ we selected HIF-1 α , VEGF, and MVD as biomarkers for neovascularization to investigate the correlation between copper and tumor angiogenesis using an IHC assay. Our findings revealed significantly decreased expression of these biomarkers following TM and/or TAE treatment compared with the control group. Moreover, the combination regimen demonstrated better inhibition of tumor growth, suppression of tumor angiogenesis, and reduction in copper concentration. Based on these results, it is concluded that TM enhances the antineoplastic activity of TAE, providing a promising avenue for clinical evaluation.

Nevertheless, this study has several limitations. While the article concludes TM enhances the antineoplastic activity of TAE, the specific underlying mechanism requires further investigation. In addition, the small sample size for each group restricts the ability to draw generalizable conclusions.

Conclusion

TM has been shown to be a highly effective antiangiogenic agent, effectively limiting angiogenesis post-TAE treatment. The combination therapy of TAE with TM represents a promising strategy and introduces a novel therapeutic method for the treatment of liver cancer.

Declarations

Ethics Approval and Consent to Participate

The study was approved by the animal ethics committee of Sun Yat-sen University (no.: SYSU-IACUC-2020-000209).

Consent for publication

NA

Author contributions

Ni Zeng: Material preparation and data collection; Data analysis; First draft of the article.

Ye Wang: Material preparation and data collection; Data analysis.

Yuan Wan: Material preparation and data collection.

Hongyu Wang: Material preparation and data collection; Data analysis; Gave critical opinions; Article revision.

Nan Li: Material preparation and data collection; Data analysis; First draft of the article.

All authors read and approved the final article.

Acknowledgements

None.

Funding

The author(s) disclosed receipt of the following financial support for the research, authorship, and/or publication of this article: This work was supported by Project of Guangzhou Municipal Health Bureau, China (grant no. 20231A011006).

Competing interests

The author(s) declared no potential conflicts of interest with respect to the research, authorship, and/or publication of this article.

Availability of data and materials

The data sets generated during and/or analyzed during this study are available from the corresponding author on reasonable request.

ORCID iD

Nan Li  <https://orcid.org/0000-0002-6100-0093>

REFERENCES

- Sung H, Ferlay J, Siegel RL, et al. Global cancer statistics 2020: GLOBOCAN estimates of incidence and mortality worldwide for 36 cancers in 185 countries. *CA: Cancer J Clin.* 2021;71:209-249.
- Llovet JM, Castet F, Heikenwalder M, et al. Immunotherapies for hepatocellular carcinoma. *Nat Rev Clin Oncol.* 2022;19:151-172.
- Llovet JM, Kelley RK, Villanueva A, et al. Hepatocellular carcinoma. *Nat Rev Dis Prim.* 2021;7:6.
- Xie DY, Ren ZG, Zhou J, Fan J, Gao Q. 2019 Chinese clinical guidelines for the management of hepatocellular carcinoma: updates and insights. *Hepatobil Surg Nutr.* 2020;9:452-463.
- Heimbach JK, Kulik LM, Finn RS, et al. AASLD guidelines for the treatment of hepatocellular carcinoma. *Hepatology (Baltimore, MD).* 2018;67:358-380.
- Vogel A, Cervantes A, Chau I, et al. Hepatocellular carcinoma: ESMO Clinical Practice Guidelines for diagnosis, treatment and follow-up. *Ann Oncol: Off J Eur Soc Med Oncol.* 2019;30:871-873.
- Finn RS, Zhu AX, Farah W, et al. Therapies for advanced stage hepatocellular carcinoma with macrovascular invasion or metastatic disease: a systematic review and meta-analysis. *Hepatology (Baltimore, MD).* 2018;67:422-435.
- Lencioni R, de Baere T, Soulen MC, Rilling WS, Geschwind JF. Lipiodol transarterial chemoembolization for hepatocellular carcinoma: a systematic review of efficacy and safety data. *Hepatology.* 2016;64:106-116.
- Wang Q, Xia D, Bai W, et al. Development of a prognostic score for recommended TACE candidates with hepatocellular carcinoma: a multicentre observational study. *J Hepatol.* 2019;70:893-903.
- Raoul JL, Sangro B, Forner A, et al. Evolving strategies for the management of intermediate-stage hepatocellular carcinoma: available evidence and expert opinion on the use of transarterial chemoembolization. *Cancer Treat Rev.* 2011;37:212-220.
- Jiang H, Meng Q, Tan H, et al. Antiangiogenic therapy enhances the efficacy of transcatheter arterial embolization for hepatocellular carcinomas. *Int J Cancer.* 2007;121:416-424.

12. Carmeliet P, Jain RK. Angiogenesis in cancer and other diseases. *Nature*. 2000;407:249-257.
13. Wang B, Xu H, Gao ZQ, et al. Increased expression of vascular endothelial growth factor in hepatocellular carcinoma after transcatheter arterial chemoembolization. *Acta Radiol (Stockholm, Sweden 1987)*. 2008;49:523-529.
14. Lloveret JM, Montal R, Sia D, Finn RS. Molecular therapies and precision medicine for hepatocellular carcinoma. *Nat Rev Clin Oncol*. 2018;15:599-616.
15. Wang Z, Dabrosin C, Yin X, et al. Broad targeting of angiogenesis for cancer prevention and therapy. *Semin Cancer Biol*. 2015;35(suppl):S224-S243.
16. Teleanu RI, Chircov C, Grumezescu AM, et al. Tumor angiogenesis and anti-angiogenic strategies for cancer treatment. *J Clin Med*. 2019;9:84.
17. da Silva DA, De Luca A, Squitti R, et al. Copper in tumors and the use of copper-based compounds in cancer treatment. *J Inorg Biochem*. 2022;226:111634.
18. Ge EJ, Bush AI, Casini A, et al. Connecting copper and cancer: from transition metal signalling to metalloplasia. *Nat Rev Cancer*. 2022;22:102-113.
19. Gupte A, Mumper RJ. Elevated copper and oxidative stress in cancer cells as a target for cancer treatment. *Cancer Treat Rev*. 2009;35:32-46.
20. Blockhuys S, Wittung-Stafshede P. Copper chaperone Atox1 plays role in breast cancer cell migration. *Biochem Biophys Res Commun*. 2017;483:301-304.
21. Jana A, Das A, Krett NL, et al. Nuclear translocation of Atox1 potentiates activin A-induced cell migration and colony formation in colon cancer. *PLoS ONE*. 2020;15:e0227916.
22. Kim Y-J, Bond GJ, Tsang T, et al. Copper chaperone ATOX1 is required for MAPK signaling and growth in BRAF mutation-positive melanoma. *Metallo: Integr Biomater Sci*. 2019;11:1430-1440.
23. Grubman A, White AR. Copper as a key regulator of cell signalling pathways. *Expert Rev Mol Med*. 2014;16:e11.
24. Nan LI, Yuan W, Guodong C, et al. Multitargeting strategy using tetrathiomolybdate and lenvatinib: maximizing anti-angiogenesis activity in a preclinical liver cancer model. *Anti-Cancer Agen Med Chem*. 2022;23:786-793.
25. Khan G, Merajver S. Copper chelation in cancer therapy using tetrathiomolybdate: an evolving paradigm. *Expert Opin Investig Drugs*. 2009;18:541-548.
26. Pan Q, Kleer CG, van Golen KL, et al. Copper deficiency induced by tetrathiomolybdate suppresses tumor growth and angiogenesis. *Cancer Research*. 2002;62:4854-4859.
27. Jain S, Cohen J, Ward MM, et al. Tetrathiomolybdate-associated copper depletion decreases circulating endothelial progenitor cells in women with breast cancer at high risk of relapse. *Ann Oncol*. 2013;24:1491-1498.
28. Chan N, Willis A, Kornhauser N, et al. Influencing the tumor microenvironment: a Phase II study of copper depletion using tetrathiomolybdate in patients with breast cancer at high risk for recurrence and in preclinical models of lung metastases. *Clin Cancer Res: Off J Am Assoc Cancer Res*. 2017;23:666-676.
29. Brewer GJ, Dick RD, Grover DK, et al. Treatment of metastatic cancer with tetrathiomolybdate, an anticopper, antiangiogenic agent: Phase I study. *Clin Cancer Res*. 2000;6:1-10.
30. Denoyer D, Clatworthy SAS, Cater MA. Copper complexes in cancer therapy. *Metal Ions Life Sci*. 2018;18:734022.
31. Kim KK, Abelman S, Yano N, et al. Tetrathiomolybdate inhibits mitochondrial complex IV and mediates degradation of hypoxia-inducible factor-1 α in cancer cells. *Sci Rep*. 2015;5:14296.
32. Lopez J, Ramchandani D, Vahdat L. Copper depletion as a therapeutic strategy in cancer. *Metal Ions Life Sci*. 2019;19:527872.
33. Marvasti TB, Alibhai FJ, Weisel RD, Li RK. CD34+stem cells: Promising roles in cardiac repair and regeneration. *Can J Cardiol*. 2019;35(10):1311-1321.
34. Liu M, Yang J, Qian S, et al. Mahuang Xixin Fuzi decoction protects the BALB/c-nude mice infected with influenza A virus by reducing inflammatory cytokines storm and weakly regulating SigA immune response. *J Ethnopharmacol*. 2023;304:116070.
35. Li N, Chen B, Lin R, et al. The earlier, the better: the effects of different administration timepoints of sorafenib in suppressing the carcinogenesis of VEGF in rats. *Cancer Chemother Pharmacol*. 2018;81:207-216.
36. Tan KV, Yang X, Chan CY, et al. Non-invasive PET/MR imaging in an orthotopic mouse model of hepatocellular carcinoma. *J Visual Exp*. 2022;186:63958.
37. Brewer GJ, Merajver SD. Cancer therapy with tetrathiomolybdate: antiangiogenesis by lowering body copper: a review. *Integr Cancer Ther*. 2002;1:327-337.
38. Fang AP, Chen PY, Wang XY, et al. Serum copper and zinc levels at diagnosis and hepatocellular carcinoma survival in the Guangdong Liver Cancer Cohort. *Int J Cancer*. 2019;144:2823-2832.
39. Weidner N, Semple JP, Welch WR, et al. Tumor angiogenesis and metastasis: correlation in invasive breast carcinoma. *N Engl J Med*. 1991;324:1-8.
40. Rhee TK, Young JY, Larson AC, et al. Effect of transcatheter arterial embolization on levels of hypoxia-inducible factor-1 α in rabbit VX2 liver tumors. *J Vasc Interv Radiol*. 2007;18:639-645.
41. Schwartz LH, Seymour L, Litière S, et al. RECIST 1.1—standardisation and disease-specific adaptations: perspectives from the RECIST Working Group. *Eur J Cancer*. 2016;62:138-145.
42. Liu K, Min XL, Peng J, Yang K, Yang L, Zhang XM. The changes of HIF-1 α and VEGF expression after TACE in patients with hepatocellular carcinoma. *J Clin Med Res*. 2016;8:297-302.
43. Marelli L, Stigliano R, Triantos C, et al. Transarterial therapy for hepatocellular carcinoma: which technique is more effective? A systematic review of cohort and randomized studies. *Cardiovasc Intervent Radiol*. 2007;30:6-25.
44. Lanza E, Donadon M, Poretti D, et al. Transarterial Therapies for Hepatocellular Carcinoma. *Liver Cancer*. 2016;6:27-33.
45. Brown KT, Do RK, Gonen M, et al. Randomized trial of hepatic artery embolization for hepatocellular carcinoma using doxorubicin-eluting microspheres compared with embolization with microspheres alone. *J Clin Oncol: Off J Am Soc Clin Oncol*. 2016;34:2046-2053.
46. Liu CH, Kuo SM, Gao HW, Hsu YJ. A rat toxicological study of intra-arterial injection of tirapazamine, a hypoxia-activating cancer therapeutic agent, followed by hepatic artery ligation. *Invest New Drugs*. 2021;39:747-755.
47. Murata S, Mine T, Sugihara F, et al. Interventional treatment for unresectable hepatocellular carcinoma. *World J Gastroenterol*. 2014;20:13453-13465.
48. Masoud GN, Li W. HIF-1 α pathway: role, regulation and intervention for cancer therapy. *Acta Pharm Sin B*. 2015;5:378-389.
49. Gao D, Xu X, Liu L, et al. Combination of pegylated-H1/HGFK1 nanoparticles and TAE in the treatment of hepatocellular carcinoma. *Appl Biochem Biotechnol*. 2022;195:505-518.
50. Huang GW, Yang LY, Lu WQ. Expression of hypoxia-inducible factor 1 α and vascular endothelial growth factor in hepatocellular carcinoma: impact on neovascularization and survival. *World J Gastroenterol*. 2005;11:1705-1708.
51. Denoyer D, Masaldan S, La Fontaine S, et al. Targeting copper in cancer therapy: "copper that cancer." *Metallo: Integr Biomater Sci*. 2015;7:1459-1476.
52. Rigraciolo DC, Scarpelli A, Lappano R, et al. Copper activates HIF-1 α /GPER/VEGF signalling in cancer cells. *Oncotarget*. 2015;6:34158-34177.
53. Finney L, Vogt S, Fukai T, Glesne D. Copper and angiogenesis: unravelling a relationship key to cancer progression. *Clin Exp Pharmacol Physiol*. 2009;36:88-94.
54. Carmeliet P, Jain RK. Molecular mechanisms and clinical applications of angiogenesis. *Nature*. 2011;473:298-307.
55. Li Y. Copper homeostasis: emerging target for cancer treatment. *IUBMB Life*. 2020;72:1900-1908.
56. Khan MK, Miller MW, Taylor J, et al. Radiotherapy and antiangiogenic TM in lung cancer. *Neoplasia*. 2002;4:164-170.
57. Moriguchi M, Nakajima T, Kimura H, et al. The copper chelator trientine has an antiangiogenic effect against hepatocellular carcinoma, possibly through inhibition of interleukin-8 production. *Int J Cancer*. 2002;102:445-452.
58. Yoshida D, Ikeda Y, Nakazawa S. Suppression of tumor growth in experimental 9L gliosarcoma model by copper depletion. *Neurol Med Chir (Tokyo)*. 1995;35:133-135.
59. Brem SS, Zagzag D, Tsanaclis AM, Gately S, Elkouby MP, Brien SE. Inhibition of angiogenesis and tumor growth in the brain. Suppression of endothelial cell turnover by penicillamine and the depletion of copper, an angiogenic cofactor. *Am J Pathol*. 1990;137:1121-1142.